

## Correspondence of unstable periodic orbits and quasi-Landau modulations

D. Wintgen

*Fakultät für Physik, Hermann-Herder-Strasse 3, D-7800 Freiburg, West Germany*

H. Friedrich

*Max-Planck-Institut für Quantenoptik, D-8046 Garching b. München, West Germany*

(Received 10 November 1986)

We study the correlation between modulations in the photoabsorption cross sections of diamagnetic Rydberg atoms and classical periodic orbits in a completely chaotic regime. Extensive quantum-mechanical calculations of photoabsorption cross sections and classical calculations of periodic trajectories are presented. In accordance with the scaling property of the classical Hamiltonian, the photoabsorption cross sections are studied for fixed values of the scaled energy  $\varepsilon = E/\gamma^{2/3}$  ( $\gamma$  is the magnetic field strength parameter) as a function of  $\gamma^{-1/3}$ . The modulations of the photoabsorption cross sections appear as prominent peaks in the Fourier-transformed cross sections and can be related to periodic classical orbits. The positions of the peaks are given quantitatively by the scaled action along the periodic orbits and the relative strengths of the peaks can be understood qualitatively by considering the geometry of the orbits and the transition involved and the stability of the classical orbits. The one-to-one correspondence between peaks in the Fourier-transformed cross sections and classical periodic orbits applies not only to the traditional quasi-Landau modulation associated with the classical orbit in the plane perpendicular to the field, but also to a large number of further modulations corresponding to topologically different series of periodic orbits. In the completely irregular region around the zero-field threshold, the unstable periodic classical orbits and the observable peaks in the modulated cross sections cannot in general be related to individual eigenstates of the quantum system.

### I. INTRODUCTION

Since the postulation of the Bohr-Sommerfeld quantum conditions in the early days of quantum mechanics, periodic classical orbits have played an important role in the theory of semiclassical quantization.<sup>1</sup> The Bohr-Sommerfeld conditions were generalized by Einstein, Brillouin, and Keller (EBK) to include nonseparable systems in which classical dynamics were regular and orbits stable in at least some fraction of phase space.<sup>2</sup>

Little is known, however, about the physical significance of *unstable* periodic orbits in a completely chaotic region of classical phase space, where neighboring trajectories diverge exponentially. A completely irregular phase space may contain a large number and even a dense set of such isolated periodic orbits, but their measure is zero. Recently Heller<sup>3</sup> showed for a free particle in a two-dimensional stadium that the existence of isolated unstable periodic orbits can lead to "scars" in corresponding quantum-mechanical wave functions, i.e., there is an accumulation of density in coordinate space near the classical trajectory.

It is becoming increasingly apparent that unstable periodic orbits are important for the understanding of the structure of diamagnetic Rydberg atoms. Many years ago Garton and Tomkins<sup>4</sup> discovered unexpected oscillatory structure in the photoabsorption cross sections of Rydberg atoms in a magnetic field. These "quasi-Landau" peaks were widely interpreted<sup>5-11</sup> as resonant photoabsorption into quantum states which were correlated to classical

periodic orbits in the plane perpendicular to the magnetic field. However, in the heart of the quasi-Landau region around the zero-field threshold the experimental data do not necessarily imply an identification of the quasi-Landau peaks as individual quantum states and it has recently been shown<sup>12</sup> that such an interpretation is at least grossly oversimplified. Nevertheless, the experimentally observed *quasi-Landau modulations* of the photoabsorption cross sections can be related to periodic orbits in the plane perpendicular to the field without invoking the existence of individual quasi-Landau quantum states, as shown by Reinhardt.<sup>13</sup> In the quasi-Landau region around the zero-field threshold the classical dynamics are known to be completely irregular<sup>14-16</sup> and the periodic orbits perpendicular to the field are unstable. (This irregularity in the classical dynamics has recently been shown to be matched by quantum level statistics expected from random matrix theories.<sup>17-19</sup>) Thus the occurrence of quasi-Landau modulations in photoabsorption cross sections is an observable manifestation of these unstable periodic orbits.

Apart from the traditional quasi-Landau modulations, which are characterized near threshold by an energy spacing roughly 1.5 times the Landau spacing of free electrons in a magnetic field, further modulations corresponding to a closer spacing have recently been seen both experimentally<sup>20,21</sup> and theoretically<sup>17</sup> and have been related to (unstable) periodic orbits outside the plane perpendicular to the field.

In this paper we present detailed classical and

quantum-mechanical studies of a hydrogen atom in a uniform magnetic field with the aim of establishing quantitatively the correspondence of modulations in the photoabsorption cross sections and classical periodic orbits. The magnetized hydrogen atom is an ideal physical system for studying the classical and quantum dynamics of nonseparable Hamiltonian systems. It is a physically real system which can be and has been prepared in the laboratory,<sup>20</sup> and the states observed experimentally correspond quantitatively to those obtained by solving the Schrödinger equation as shown recently in a state-for-state comparison between calculation and experiment.<sup>22</sup> Despite its apparent simplicity it is complex enough to display the essential features of a nonintegrable system, including the transition from regularity to irregularity, which is manifest both in the classical trajectories<sup>14-16</sup> and in the corresponding quantum level distributions.<sup>17-19,23</sup>

In Sec. II we discuss the classical and quantum-mechanical equations of motion for a hydrogen atom in a uniform magnetic field and, in particular, our method of solving the Schrödinger equation (Sec. II B). Because of the scaling properties of the classical Hamiltonian, the classical dynamics depend not on the energy  $E$  and field strength  $\gamma$  independently, but only on the scaled energy  $\varepsilon = E/\gamma^{2/3}$ . Modulations of the photoabsorption cross sections are best revealed by studying Fourier-transformed cross sections at fixed  $\varepsilon$  (Sec. II D). The results of our calculations are presented in Sec. III. Photoabsorption cross sections are calculated for various scaled energies and for different subspaces of final states. Periodic classical orbits are found in a systematic way. In addition to the set of periodic orbits found by Main *et al.*<sup>21</sup> we find further periodic orbits, some of which are important for understanding the photoabsorption cross sections. The modulations of the photoabsorption cross sections appear as prominent peaks in the Fourier-transformed spectra and the positions of these peaks can be related to a scaled action of the classical periodic orbits. At the zero-field threshold  $\varepsilon=0$ , we give a complete account of all periodic orbits passing through the origin with a scaled action less than four. For all peaks observed in the Fourier-transformed spectra, we can identify a classical periodic orbit whose scaled action gives the position of the peak to an accuracy better than 1%. The relative heights of the peaks can be explained by qualitative arguments based on the geometry of the transition and of the classical orbits, and on the stability of the classical orbits. The calculations are all done for the simple hydrogen atom, but it is obvious that a region of normal atomic dimensions is not important because the spatial dimensions of the quantum wave functions and classical trajectories we study are typically of the order of thousands of Bohr radii; hence the essential features of the results, which are summarized and discussed in Sec. IV, are applicable to diamagnetic Rydberg atoms in general.

## II. THEORY AND METHOD

### A. Scaling property of the classical system

A hydrogen atom in a uniform magnetic field (parallel to the  $z$  axis) is accurately described by a one-electron

Hamiltonian  $H$ , which, in the frame of reference rotating with the Larmor frequency about the  $z$  axis, is (in Rydberg units)

$$H = p_\rho^2 + p_z^2 + \frac{l_z^2}{\rho^2} - \frac{2}{r} + \frac{\gamma^2}{4}\rho^2, \quad (1)$$

where  $\gamma$  is the field strength measured in units of  $B_0 \approx 2.35 \times 10^5$  T.

The classical equations of motion are invariant under the following transformation:

$$\begin{aligned} \tilde{\rho} &= \gamma^{2/3}\rho, & \tilde{z} &= \gamma^{2/3}z, \\ \tilde{p}_\rho &= \gamma^{-1/3}p_\rho, & \tilde{p}_z &= \gamma^{-1/3}p_z, \\ \tilde{t} &= \gamma t, & \tilde{l}_z &= \gamma^{1/3}l_z, \end{aligned} \quad (2)$$

and are governed by the scaled Hamiltonian

$$\tilde{H} = \tilde{p}_\rho^2 + \tilde{p}_z^2 + \frac{\tilde{l}_z^2}{\tilde{\rho}^2} - \frac{2}{\tilde{r}} + \frac{1}{4}\tilde{\rho}^2 = H/\gamma^{2/3}, \quad (3)$$

which no longer depends on the field strength. The scaled angular momentum  $\tilde{l}_z$  in (3) is negligibly small under laboratory conditions.

The immediate consequence of the scaling property (2), (3) is that all properties of the classical system do not depend on the energy  $E$  and field strength  $\gamma$  independently but only on the scaled energy  $\varepsilon = E/\gamma^{2/3}$ .

### B. The Schrödinger equation

The quantum-mechanical one-electron Schrödinger equation for the magnetized hydrogen atom is (again in Rydberg units)

$$(-\Delta - 2/r + \frac{1}{4}\gamma^2\rho^2)\psi(\mathbf{r}) = E\psi(\mathbf{r}). \quad (4)$$

It is of considerable practical advantage<sup>24,25</sup> to introduce semiparabolic coordinates (although the scaling properties described below are quite general)

$$\mu = (r+z)^{1/2}, \quad \nu = (r-z)^{1/2}. \quad (5)$$

In the subspace of states with a given value  $m$  of the conserved azimuthal quantum number, the Schrödinger equation now reads

$$[\Delta_\mu + \Delta_\nu + E(\mu^2 + \nu^2) - \frac{1}{4}\gamma^2(\mu^4\nu^2 + \mu^2\nu^4) + 4]\psi(\mu, \nu) = 0, \quad (6)$$

where  $\Delta_\mu$  and  $\Delta_\nu$  are the Laplacians for the *radial parts*  $\mu$ ,  $\nu$  of two two-dimensional coordinates at fixed azimuthal quantum number  $m$ , e.g.,

$$\Delta_\mu = \frac{1}{\mu} \frac{\partial}{\partial \mu} \mu \frac{\partial}{\partial \mu} - \frac{m^2}{\mu^2}. \quad (7)$$

Apart from the azimuthal quantum number  $m$ , the only good quantum number is the  $z$  parity  $\pi$ , which manifests itself in Eq. (6) by the invariance with respect to interchanging  $\mu$  and  $\nu$ . The Schrödinger equation is not separable in any coordinate system, and Eq. (6) is one of many equivalent formulations for this nonseparable problem in two variables.

Various methods of solving Eq. (6) reflecting various scaling properties can be formulated transparently if we take matrix elements in a basis of (parity-projected) harmonic-oscillator states characterized by a given oscillator width  $b$ . Equation (6) thus becomes

$$\left[ -\frac{1}{b^2} \tilde{T} + Eb^2 \tilde{V}_{\text{HO}} - \frac{1}{4} \gamma^2 b^6 \tilde{V}_B + 4 \right] \psi = 0, \quad (8a)$$

where  $\tilde{T}$ ,  $\tilde{V}_{\text{HO}}$ , and  $\tilde{V}_B$  are all sparse banded matrices of the operators  $-\Delta_\mu - \Delta_\nu$ ,  $\mu^2 + \nu^2$ , and  $\mu^4 \nu^2 + \mu^2 \nu^4$ , respectively. The elements of these matrices are pure dimensionless numbers independent of  $E$ ,  $b$ , and  $\gamma$ .

There are different meaningful ways of solving Eq. (8a).

*Method A.* Dividing by  $-b^2$  and putting the term with the oscillator potential matrix  $\tilde{V}_{\text{HO}}$  onto the right-hand side gives

$$(1/b^4 \tilde{T} + \frac{1}{4} \gamma^2 b^4 \tilde{V}_B - 4/b^2) \psi = E \tilde{V}_{\text{HO}} \psi. \quad (8b)$$

For fixed values of the field strength  $\gamma$  and the oscillator width  $b$ , Eq. (8b) represents a *generalized* eigenvalue problem and can be solved by standard procedures for diagonalizing matrices in a nonorthogonal representation. Solving (8b) yields the energy spectrum at fixed field strength  $\gamma$ . This method is exactly equivalent to the Sturmian approach used by other authors,<sup>26-29</sup> the quantity  $2/b^2$  plays the role of the Sturmian parameter<sup>27</sup>  $\xi$ .

*Method B.* Multiplying Eq. (8a) by  $(-b^2)$  and putting the constant term onto the right-hand side gives

$$(\tilde{T} - Eb^4 \tilde{V}_{\text{HO}} + \frac{1}{4} \gamma^2 b^8 \tilde{V}_B) \psi = 4b^2 \psi. \quad (8c)$$

For a fixed value  $\delta$  of  $Eb^4$  and a fixed value  $\lambda$  of  $\gamma b^4$ , Eq. (8c) represents a *standard* eigenvalue problem for the oscillator widths  $b$ . Each eigenstate has its own oscillator width  $b$  and corresponds to a solution of the Schrödinger equation with energy  $E = \delta/b^4$  at the field strength  $\gamma = \lambda/b^4$ . This method generates spectra along lines of constant  $E/\gamma = \delta/\lambda$  and has been used in large-scale calculations<sup>12,17,22-25</sup> to solve the Schrödinger equation over large areas in the  $E - \gamma$  plane. This method has also been used<sup>24</sup> as a starting point for the explicit construction of an approximately separable representation of the Schrödinger equation and for the definition of an approximately conserved separation index  $K$  for negative energies  $E$ .

*Method C.* Choosing  $b = \gamma^{-1/3}$  and putting the kinetic energy matrix onto the right-hand side, Eq. (8a) becomes

$$(E\gamma^{-2/3} \tilde{V}_{\text{HO}} - \frac{1}{4} \tilde{V}_B + 4) \psi = \gamma^{2/3} \tilde{T} \psi. \quad (8d)$$

For fixed values of  $E\gamma^{-2/3} = \varepsilon$ , Eq. (8d) represents a *generalized* eigenvalue problem for the field strengths  $\gamma^{2/3}$ . This method generates spectra along lines of constant scaled energy  $\varepsilon$  which is precisely the quantity that controls the classical dynamics governed by the scaled classical Hamiltonian (3). Thus Eq. (8d) is the natural starting point for a comparison between the classical and the quantum-mechanical aspects of the magnetized hydrogen atom.<sup>23</sup>

There are still other possible methods of solving Eq. (8a) and which generate spectra, e.g., for constant energy

or on lines of constant  $E\gamma^{-4/3}$ . The results in this paper have been obtained with methods *B* and *C*. If one is interested in the field strength dependence of the spectrum, method *B* provides the most efficient algorithm, mainly because solving the eigenvalue problem for the oscillator widths  $b$  ensures that eigenstates in each part of the spectrum are given in terms of an optimally adjusted basis. In fact, method *B* is much more efficient than the Sturmian method *A*, where the fixed oscillator width  $b$  in each diagonalization means that the basis states are only well adjusted to a small section of the spectrum. Nevertheless, method *A* may be useful if one is interested in the spectrum for an isolated fixed field strength.

### C. Correspondence between the classical and quantum-mechanical systems

The classical dynamics governed by the Hamiltonian (3) have been studied in detail in the literature.<sup>14-16</sup> Below a critical value  $\varepsilon_c$  of the scaled energy, the motion of the electron is regular for all initial conditions and an approximate third integral of motion has been used for semiclassical quantization.<sup>30,31</sup> For small values of the scaled angular momentum, the critical scaled energy is  $\varepsilon_c \approx -1.0$ . For (scaled) energies above  $\varepsilon_c$ , the system becomes increasingly chaotic until it behaves completely random near and above the zero-field threshold  $E = \varepsilon = 0$ , where regular parts of phase space have negligible measure.

Regularity and irregularity of the classical dynamics are reflected in the energy-level spectra of the quantum system. Well below threshold the Schrödinger equation is approximately separable<sup>24</sup> and this leads to approximate level crossings first noticed by Zimmerman *et al.*<sup>32</sup> Approximate separability breaks down near the zero-field threshold and this is reflected in the nearest-neighbor spacings of the levels which accurately follow<sup>17</sup> a Wigner distribution as expected from random matrix theories. In fact, the turnover in the quantum level statistics has recently been shown<sup>23</sup> to correspond quite closely to the relatively sudden drop in the regular fraction of available classical phase space which occurs around  $\varepsilon = -0.7$  for small values of  $\tilde{I}_z$ . For  $\varepsilon \gtrsim -0.2$  the system is completely irregular, both classically and quantum mechanically.

### D. Quasi-Landau modulations

Despite the irregularity of the quantum level spectra around the zero-field threshold,<sup>17</sup> experimentally observed photoabsorption cross sections show remarkably regular modulations, as first discovered in magnetized barium by Garton and Tomkins<sup>4</sup> and recently seen also in atomic hydrogen by Holle *et al.*<sup>20</sup> The original quasi-Landau modulations are characterized at fixed field strength by an energy spacing of roughly 1.5 times the Landau spacing of free electrons in a magnetic field. These quasi-Landau modulations have long been associated with the (periodic) classical motion of the electron in the plane perpendicular to the magnetic field, but it is now apparent that the simple interpretation of the quasi-Landau peaks as resonant photoabsorption into individual quantum states is incorrect,<sup>12</sup> even though a semiclassical quantization of the

classical periodic orbits mentioned above does give the right energy spacings.

A different interpretation of the quasi-Landau modulations has been given by Reinhardt,<sup>13</sup> who argues that the recurrence of a wave packet moving along a classical trajectory induces oscillatory structure in the Fourier transform of the dipole autocorrelation function and hence in the photoabsorption cross sections. (See also Heller.<sup>33</sup>)

Recently, further modulations corresponding to a closer spacing of peaks in the  $E$ - $\gamma$  plane have been observed both experimentally<sup>20,21</sup> and theoretically,<sup>17</sup> and have been related to classical periodic orbits outside the plane perpendicular to the field. These classical periodic orbits are unstable and isolated in a classically chaotic regime. There exists a semiclassical theory, formulated by Gutzwiller, Balian and Bloch, and Berry which connects the actions of these orbits with oscillating contributions to the semiclassical level density;<sup>1</sup> this theory has recently been verified<sup>34</sup> for the diamagnetic Rydberg problem. The modulations can be interpreted as a result of the constructive interference that occurs when the electron returns to its starting point in phase and this leads to the "resonance condition"

$$\frac{1}{h} \int \mathbf{p} d\mathbf{r} = n. \quad (9)$$

Note that the interpretation of Eq. (9) as a quantization condition is only justified for isolated stable periodic orbits.<sup>1</sup> The more general resonance condition (9) will be applied in particular to unstable periodic orbits and will in general not define individual eigenstates of the quantum system, but a clustering of levels on a scale larger than the mean level spacing.<sup>1,34</sup> Equation (9) can be expressed in terms of the scaled coordinates and momenta (2)

$$\gamma^{-1/3} S(\epsilon) = n, \quad (10)$$

where

$$S(\epsilon) = \frac{1}{h} \int \bar{p} d\bar{r} \quad (11)$$

is the scaled action along the closed trajectory and depends only on the scaled energy  $\epsilon = E\gamma^{-2/3}$  and not on  $E$  and  $\gamma$  separately.

Equation (10) can be rewritten as

$$En^2 = (n\gamma^{1/3})^2 S^{-1}(n\gamma^{1/3}), \quad (12)$$

where  $S^{-1}$  is the inverse function of the scaled action. Equation (12) states that  $En^2$  is purely a function of  $\gamma n^3$ , a result assumed by Feneuille<sup>35</sup> for the traditional quasi-Landau peaks. We now see that such a scaling property holds for the modulation peaks related to any periodic orbit. It is also clear that the modulation peaks are, for any fixed value of the scaled energy  $\epsilon$ , equidistant on a scale proportional to  $\gamma^{-1/3}$ . Hence, instead of studying the photoabsorption cross sections as a function of energy (at fixed  $\gamma$ ) and the Fourier-transformed spectra in the time domain, it is most appropriate to investigate the modulations by studying the photoabsorption cross sections at fixed scaled energy  $\epsilon$  as functions of  $\gamma^{-1/3}$ . In this representation the classical dynamics are independent of the variable and the spacing of the (expected) modulation

peaks becomes constant. The Fourier-transformed spectra are now not in the time domain but are functions of a variable conjugate to  $\gamma^{-1/3}$ ; we call this variable  $\gamma^{+1/3}$  for simplicity.

### III. RESULTS

In this section we present the results of elaborate quantum-mechanical calculations obtained with the methods described in Sec. II and relate the modulations of photoabsorption cross sections to periodic orbits obtained by numerical integration of the classical equations of motion.

An example of photoabsorption cross sections is shown in Fig. 1 where we plot the renormalized oscillator strengths  $f\nu^3$  for Balmer transitions into the  $m^\pi = -1^-$  and  $m^\pi = -2^+$  subspaces at the zero-field threshold  $E = \epsilon = 0$ . The effective quantum number  $\nu$  is defined relative to the real ionization threshold which lies  $(|m| + 1)\gamma$  Ry above  $E = 0$ . Eigenvalues and eigenvectors were calculated by diagonalizing banded matrices with dimensions up to 3136 using method *B* described in Sec. II B. The abscissa is linear in  $\gamma^{-1/3}$ , because the quasi-Landau modulations are uniform on this scale, as

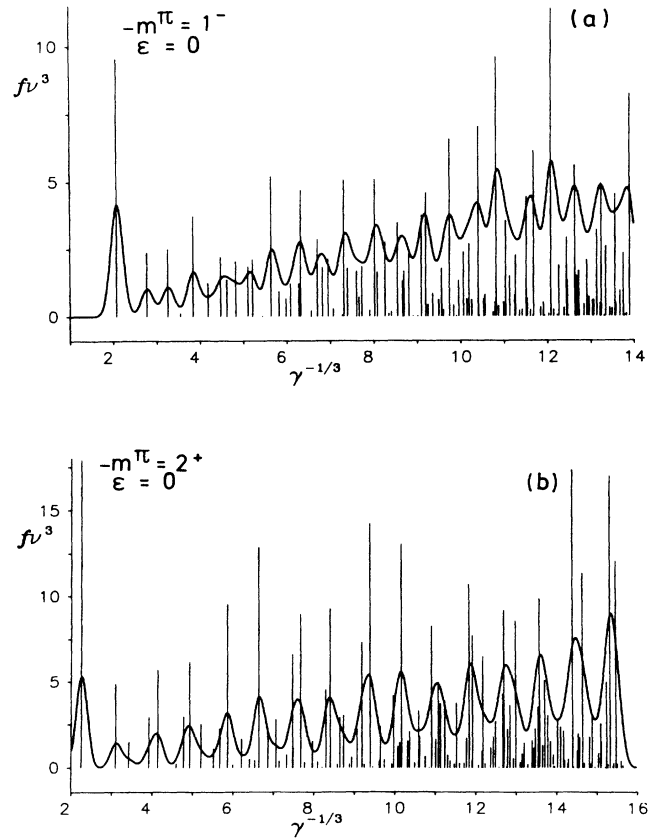


FIG. 1. Photoabsorption spectra at the zero-field threshold for  $\Delta m = 0$  Balmer transitions into the  $m^\pi = -1^-$  subspace (a), and for  $\Delta m = -1$  Balmer transitions into the  $m^\pi = -2^+$  subspace (b). The solid curves show the cross sections obtained by Gaussian smearing of the oscillator strengths.

discussed in Sec. II D. Note that the uniformly spaced modulation peaks are not generally related to uniformly spaced individual quantum states. The fact that one modulation peak encompasses a whole bunch of quantum states becomes increasingly apparent towards the denser part of the spectrum (see also Ref. 12). The modulations of the photoabsorption cross sections are revealed in the respective Fourier transforms shown in Figs. 2(a) and 2(b). The Fourier spectra are rather simply structured and dominated by a few peaks only. The leading modulation in the original cross sections (Fig. 1) corresponds to the first peak in the Fourier transform (i.e., the one at the smallest value of  $\gamma^{1/3}$ ) and can be made visible by a Gaussian smearing of the oscillator strengths. This is shown by the thick solid lines in Fig. 1 which thus simulate an experimental situation with poor resolution.

The integration of the classical equations of motion was done in semiparabolic coordinates defined as in Eq. (5). This procedure has the advantage that the equations of motion are no longer singular at the origin. Since photoabsorption takes place near the origin only those trajectories which pass through the origin (or very close to the origin) are important. For this reason the centrifugal term in the equations of motion can be neglected. Periodic orbits were found by starting a trajectory at the origin and looking for orbits which return to the origin after a given recurrence time  $t_{\text{rec}}$ . Each such orbit is periodic. A search is made by varying the initial value of  $\dot{\mu}/\dot{\nu}$  which

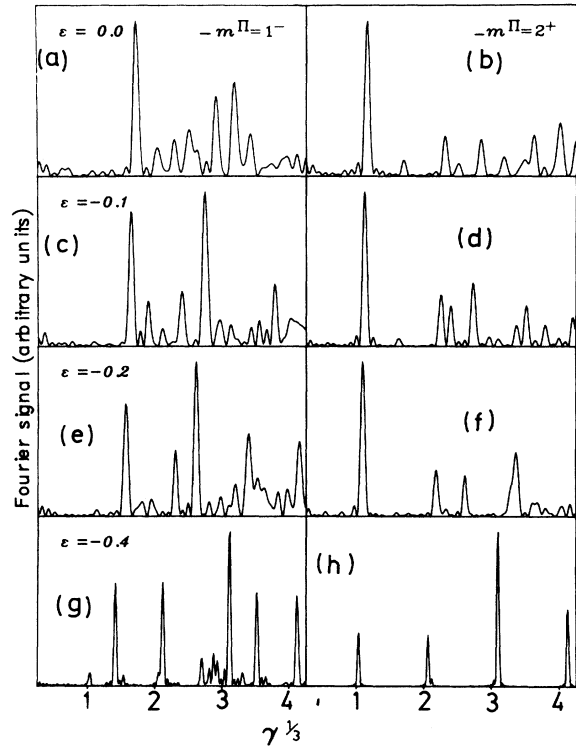


FIG. 2. Fourier-transformed photoabsorption spectra for various values of the scaled energy  $\epsilon$ .

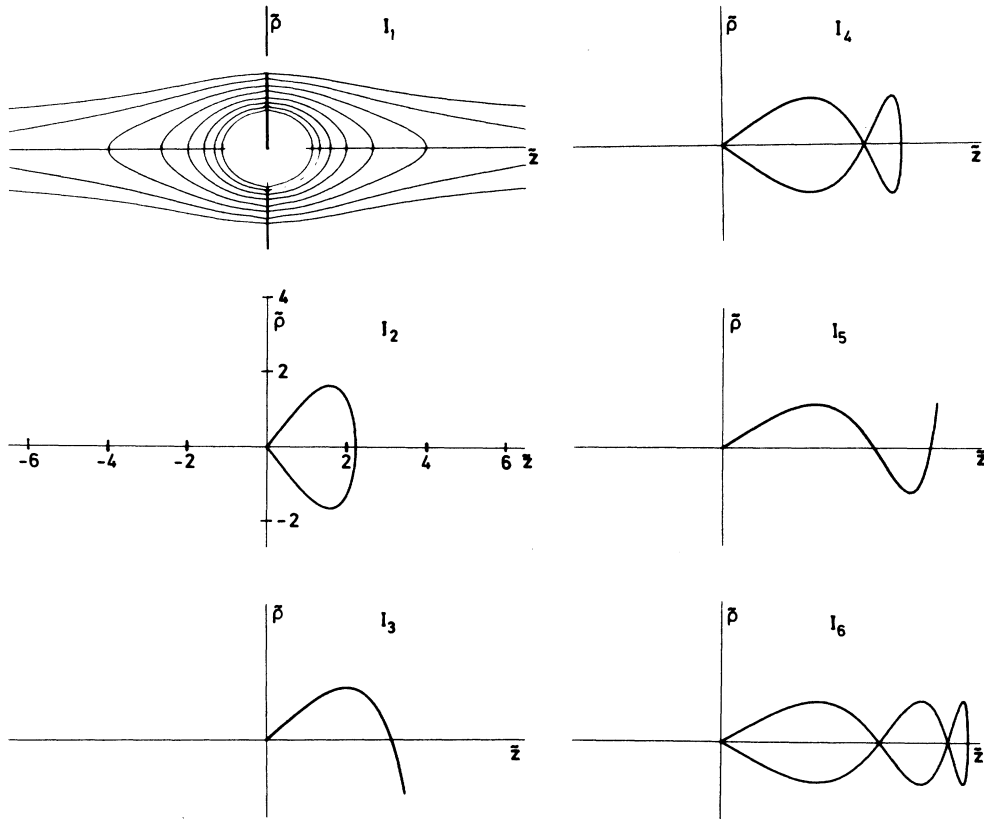


FIG. 3. Leading members of series I of classical periodic orbits at  $\epsilon=0$ . The diagram showing the first member  $I_1$  of the series, perpendicular to the  $z$  axis, also shows the equipotential lines. The scale is shown in the diagram for  $I_2$  and is the same throughout the figure.

determines the initial angle  $\theta = \lim_{t \rightarrow 0} \arctan[\rho(t)/z(t)]$  of the trajectory in the  $\rho$ - $z$  plane. By systematically varying the initial value of  $\dot{\mu}/\dot{\nu}$  between zero and unity we obtain *all* periodic orbits which pass through the origin.

At the zero-field threshold we calculated *all* periodic orbits passing through the origin with a scaled action  $S(\varepsilon=0)$  less than four. Our calculations show several sets of topologically different orbits and are illustrated in Figs. 3–6. Since we are neglecting the (cylindrical) centrifugal potential, the orbits all lie in a plane through the  $z$  axis. Figure 3 shows the first members of a series of Lissajous-type periodic orbits recently studied by Main *et al.*<sup>21</sup> In this series, which we call series I, the orbits are characterized by the number  $n = 1, 2, 3, \dots$  where  $n - 1$  is the number of times the orbit crosses the  $z$  axis between its start at and first recurrence to the origin. At

their maximum  $z$ -value, orbits with odd  $n$  are reflected at the sides of the potential valley and retrace their path in coordinate space, while orbits with even  $n$  cross the  $z$  axis at right angles. The first orbit  $I_1$  in this series is the orbit in the plane perpendicular to the field and has long been associated with the traditional quasi-Landau modulations.

Figure 4 shows *all* members of a topologically different set of periodic orbits which always meet the  $z$  axis and the walls of the potential valley at skew angles. We call this series IIa. Figure 5 shows all members of a further series (series IIb) of orbits, which, except for the first member IIb<sub>0</sub>, are topologically very similar to the orbits in series IIa. Finally, Fig. 6 shows other periodic orbits which belong to different series topologically, but which we shall group together as series III.

Table I lists all the periodic orbits shown in Figs. 3–6

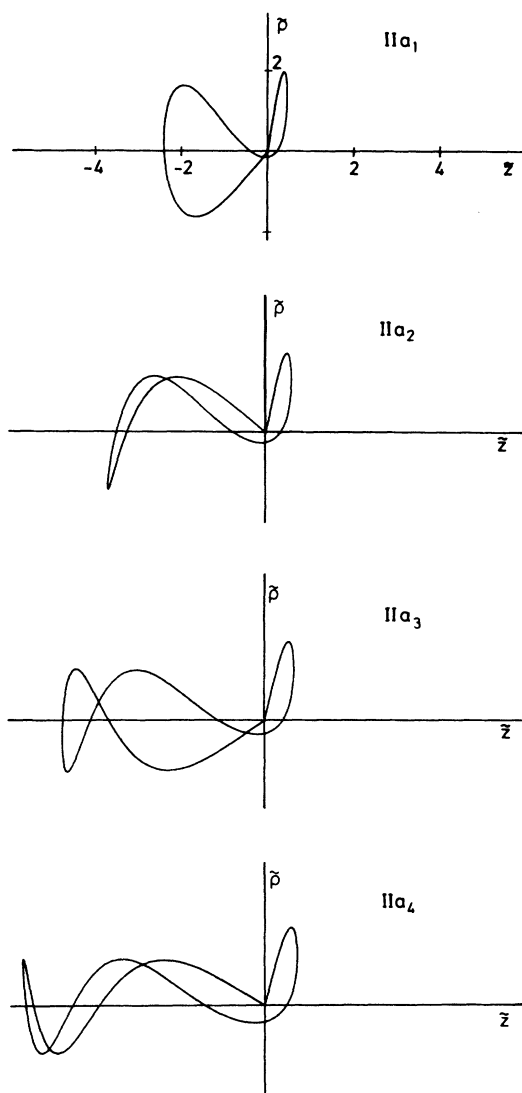


FIG. 4. All members of the series IIa of periodic orbits at  $\varepsilon=0$ . The scale is shown in the first diagram and is the same throughout the figure.

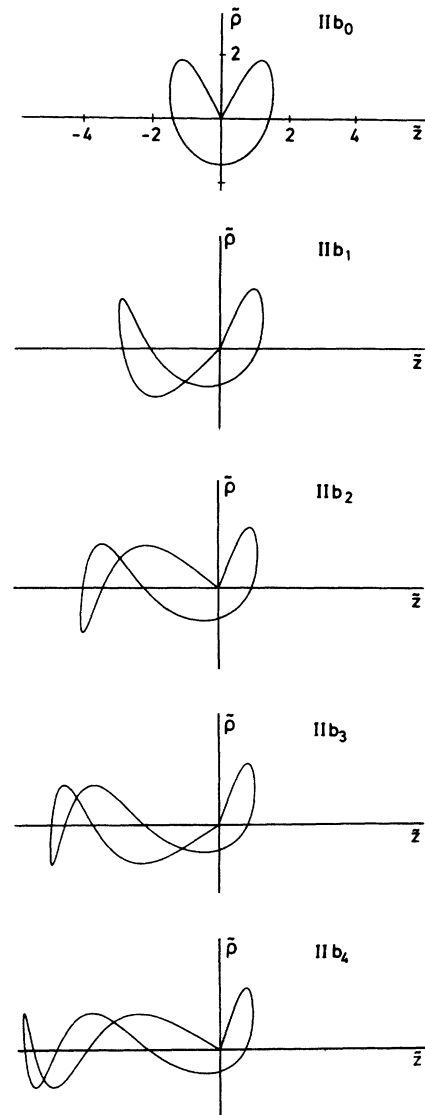


FIG. 5. All members of the series IIb of periodic orbits at  $\varepsilon=0$ . The scale is shown in the first diagram and is the same throughout the figure.

TABLE I. Table of periodic orbits (PO) shown in Figs. 3–6.  $\theta$  is the initial angle in degrees,  $t_{\text{rec}}$  the recurrence time in units of the cyclotron time for  $\varepsilon=0$ ,  $S$  the values of integral defined by Eq. (11). For  $\varepsilon \neq 0$  only the larger initial angle is given. The Coulomb orbit noted in the last line corresponds to the motion parallel to the field.

PO	$t_{\text{rec}}$	$\varepsilon=0$		$\varepsilon=-0.1$		$\varepsilon=-0.2$		$\varepsilon=-0.4$	
		$\theta$	$S$	$\theta$	$S$	$\theta$	$S$	$\theta$	$S$
I <sub>1</sub>	0.67	90.0	1.16	90.0	1.13	90.0	1.09	90.0	1.03
I <sub>2</sub>	1.57	53.8	1.72	51.0	1.64	47.8	1.56	39.9	1.41
I <sub>3</sub>	2.58	42.8	2.05	39.2	1.92	35.0	1.79	23.1	1.54
I <sub>4</sub>	3.59	37.3	2.29	33.2	2.11	28.1	1.93	10.5	1.58
I <sub>5</sub>	4.60	33.8	2.49	29.2	2.26	23.3	2.03		
IIb <sub>0</sub>	2.15	63.7	2.51	62.2	2.41	60.7	2.31	58.4	2.12
I <sub>6</sub>	5.61	31.4	2.66	26.3	2.38	19.7	2.10		
I <sub>7</sub>	6.61	29.5	2.81	24.1	2.48	16.5	2.15		
IIa <sub>1</sub>	2.36	[81.7 51.7]	2.85	78.9	2.74	74.2	2.61		
IIb <sub>1</sub>	3.04	[67.5 46.7]	2.91	67.0	2.76	67.7	2.62		
IIa <sub>2</sub>	3.46	[79.1 41.5]	3.16	74.7	2.99				
IIb <sub>2</sub>	3.99	[69.5 39.6]	3.19	70.5	2.99				
III <sub>1</sub>	2.89	60.3	3.24	58.0	3.10	55.5	2.96	49.4	2.69
IIa <sub>3</sub>	4.55	[77.5 36.3]	3.40						
IIb <sub>3</sub>	4.93	[71.0 35.4]	3.40						
IIa <sub>4</sub>	5.63	[76.1 33.0]	3.59						
IIb <sub>4</sub>	5.86	[72.4 32.6]	3.59						
III <sub>2</sub>	3.87	[59.2 45.2]	3.61	56.8	3.42	53.9	3.23	46.5	2.87
III <sub>3</sub>	2.87	[83.8 64.2]	3.66	81.9	3.52	79.2	3.38		
III <sub>4</sub>	3.59	66.2	3.75	65.1	3.57	64.3	3.41	66.2	3.11
III <sub>5</sub>	4.16	[54.5 42.6]	3.77	51.8	3.56	48.9	3.35	42.9	2.94
III <sub>6</sub>	4.86	[58.7 38.7]	3.87	56.1	3.63	53.1	3.40	44.2	2.94
III <sub>7</sub>	3.19	81.2	3.98	78.0	3.82				
III <sub>8</sub>	3.54	61.3	3.99	59.4	3.81	57.2	3.64	52.7	3.33
III <sub>9</sub>	3.05	[87.8 51.6]	4.01	86.3	3.86				
Coulomb	$\infty$	0	$\infty$	0	3.16	0	2.24	0	1.58

together with the initial angles  $\theta$  in the  $\rho$ - $z$  plane and the recurrence times  $t_{\text{rec}}$ . Note that, in numerical applications, the initial conditions generally have to be defined much more accurately than the values of  $\theta$  given in the table in order to ensure recurrence to the origin. This is characteristic of a classically chaotic regime where small errors propagate exponentially.

If we study the photoabsorption cross sections at fixed field strength  $\gamma$ , then the modulations which appear as peaks in the Fourier-transformed spectra are correlated to the recurrence times of the periodic orbits<sup>1</sup>

$$\Delta E = h \left[ \frac{d}{dE} [\gamma^{-1/3} S(\varepsilon)] \right]^{-1} = h (T_{\text{rec}}/\gamma)^{-1} = h/t_{\text{rec}}, \quad (13)$$

where  $t_{\text{rec}}$  is the period of the orbit in cyclotron units.

Since we are, as explained in Sec. II d, studying the photoabsorption cross sections as functions of  $\gamma^{-1/3}$  at fixed scaled energies  $\varepsilon$ , we expect correlations between the peaks  $\gamma_i^{1/3}$  in the Fourier-transformed spectra and the values of the scaled action  $S_i$  of the periodic orbits.

We now study in detail the Fourier spectra of Fig. 2 in connection with the periodic orbits tabulated in Table I. We first take the Fourier spectra for  $m^\pi = -2^+$  and  $\varepsilon=0$  [Fig. 2(b)]. Table II lists the positions  $\gamma_i^{1/3}$  of the Fourier peaks together with the corresponding periodic orbits from Table I which we believe to be responsible for the Fourier peak. The positions of the first two peaks at 1.15 and 1.70 can be unambiguously connected with the first two members of series I. However, the amplitude of the second peak is only small and, moreover, the third member of the series, for which we would expect a peak near  $\gamma^{1/3}=2.05$ , is completely absent. This can be under-

TABLE II. Observed positions  $\gamma_i^{1/3}$  of the calculated peaks in the Fourier spectra of Figs. 2(a) and 2(b) for  $\epsilon=0$ , together with the associated periodic orbit and the corresponding value  $S$ . Parentheses indicate poorly resolved peaks (columns 1,2) or (columns 3,4) further orbits which may be correlated with the observed peaks.

$m^\pi=2^+$	$\gamma_i^{1/3}$	$m^\pi=1^-$	$S_i$	Periodic orbit
1.15			1.16	I <sub>1</sub>
1.70		1.71	1.72	I <sub>2</sub>
		2.04	2.05	I <sub>3</sub>
		2.29	2.29	I <sub>4</sub>
2.31			$2 \times 1.16$	I <sub>1</sub>
2.51		2.50	2.49, 2.51	I <sub>5</sub> , IIb <sub>0</sub>
		(2.63)	2.66	I <sub>6</sub>
2.84		2.91	2.85	IIa <sub>1</sub>
			2.91	IIb <sub>1</sub>
3.18		3.19	3.16, 3.19	IIa <sub>2</sub> , IIb <sub>2</sub>
3.48		3.42	$2 \times 1.72$	I <sub>2</sub>
			3.40	IIb <sub>3</sub> , IIa <sub>3</sub>
3.62			3.61, (3.59, 3.59, 3.66)	III <sub>2</sub> , (IIa <sub>4</sub> , IIb <sub>4</sub> , III <sub>3</sub> )
4.00			3.99, 3.99, 4.01	III <sub>7</sub> , III <sub>8</sub> , III <sub>9</sub>

stood by the geometry of the transition: the calculated oscillator strengths are proportional to the squared dipole matrix elements with a  $|2p, m=-1\rangle$  initial state. Due to the dipole selection rules, the  $\Delta m = -1$  transition matrix elements are then sensitive to the ( $l=2, m=-2$ ) contributions of the final state wave functions only. However, the associated Legendre polynomial  $P_2^2$  is proportional to  $\sin^2\theta$  and we expect that peaks in the Fourier spectra are largely suppressed if the initial angles  $\theta_i$  of the periodic orbits become small. Conversely, periodic orbits with large initial angles (near  $90^\circ$ ) should appear as enlarged peaks in the Fourier spectra. Only the initial angle is of interest, because the hydrogen  $2p$  states as initial states in the transition matrix elements are localized within a few Bohr radii of the origin, whereas the periodic orbits shown in Figs. 3–6 may reach some thousands Bohr radii. The absence of the peak at  $\gamma^{1/3}=2.05$  is a special property of the transition involved and *does not* mean that the modulation of the level density caused by the corresponding closed orbit is absent.<sup>34</sup>

The next peak occurs at  $\gamma^{1/3}=2.31$ . Although it could be related to the orbit I<sub>4</sub> with  $S=2.29$ , we will rule out this possibility because of the argument above. Moreover, we will rule out any orbit of I<sub>n</sub> with  $n \geq 3$ . It is more likely that the peak at 2.31 is an artifact of the Fourier procedure and is caused by the dominant modulation I<sub>1</sub> via period doubling. Such peaks with multiple values of lower Fourier peaks can occur whenever the modulations in the original spectra deviate from a sinelike modulation, which is obviously the case as can be seen in Fig. 1(b). The period-doubled peak can be viewed as generated by a repeated traversal of the periodic orbit.<sup>1,34</sup> The identification of the next two peaks at  $\gamma^{1/3}=2.51$  and 2.84 with the periodic orbits IIb<sub>0</sub> and IIa<sub>1</sub> is unambiguous. Note that the orbit IIa<sub>1</sub> has a large initial angle  $\theta=81.7^\circ$  and the amplitude of the corresponding peak is rather large.

Further peaks at  $\gamma_i^{1/3}=3.18, 3.48, 3.62$ , and 4.00 may be related to other orbits listed in Table I, but the assignment is not unique. It also may be that two or more periodic orbits with very similar values of  $S$  contribute to an unresolved single peak in the Fourier spectrum. However, we point out that no peak is observed which cannot be connected with a periodic orbit taken from Table I; the  $S$  values listed in Table I are not so dense that this is a trivial observation.

We now turn to the Fourier spectrum of the  $\Delta m=0$  Balmer transition into the  $m^\pi=-1^-$  subspace of states shown in Fig. 2(a). The peak positions  $\gamma_i^{1/3}$  are also listed in Table I. The situation is somewhat different because the dipole matrix elements are now sensitive to the ( $l=2, m=-1$ ) contribution in the final-state wave functions only. The associated Legendre polynomial  $P_2^1$  is proportional to  $\sin\theta \cos\theta$  and from the discussion above we now expect that Fourier peaks associated with periodic orbits with initial angles around  $45^\circ$  are enlarged, while peaks associated with orbits with large or small initial angles are suppressed. This explains why the peak belonging to the orbit I<sub>1</sub> with  $\theta=90^\circ$  is absent in Fig. 2(a) [Note: not only does the ( $l=2, m=-1$ ) contribution in the final wave functions vanish for  $\theta=90^\circ$ , but the whole wave functions vanish identically at  $\theta=90^\circ$  because of the negative  $z$  parity of these states]. Note that the extent to which recurrence of a classical trajectory induces oscillations in the photoabsorption cross section depends also on the Liapunov exponent<sup>34</sup> which determines the rate of exponential divergence of neighboring trajectories.<sup>36</sup> Thus a quantitative account of the relative heights of the peaks in the Fourier-transformed spectra requires an additional analysis of the degree of instability of the various periodic orbits.

The first Fourier peaks arise at  $\gamma_i^{1/3}=1.71, 2.04, 2.29$ , and 2.50 and are in excellent agreement with the members from series I with  $S_i=1.72, 2.05, 2.29$ , and 2.49. The or-

bit  $I\text{I}b_0$  with  $S = 2.51$  may however also contribute to the peak at 2.50. Another peak seems to lie near  $\gamma^{1/3} = 2.63$  but it is not fully resolved so that it may really lie near a larger value of  $\gamma^{1/3}$  in agreement with  $S = 2.66$  for  $I_6$ . The next peak at  $\gamma^{1/3} = 2.91$  can safely be connected with the  $I\text{I}b_1$  orbit.

Note the very nice agreement between the 2.84, 2.91 peaks in the  $m^\pi = 2^+, 1^-$  subspace and the periodic orbits with scaled actions 2.85, 2.91 and initial angles of  $81.7^\circ, 46.7^\circ$ . A further strong peak occurs at  $\gamma^{1/3} = 3.19$  and we believe that both the  $I\text{I}b_2$  and  $I\text{I}a_2$  orbits contribute to this peak. Before we discuss the dependence of the Fourier spectra and the classical trajectories on  $\varepsilon$ , we will turn to a short discussion of the experimental data available to date.<sup>20,21</sup>

For the  $m^\pi = -2^+$  subspace there is only one Fourier spectrum, taken at a fixed field strength, available [see Fig. 2(c) of Holle *et al.*<sup>20</sup>]. The leading modulation  $\gamma^{1/3} = 1.16$  is present in the experimental data as indicated by the peak at  $t_{\text{rec}} = 0.67$  cyclotron units, which corresponds to the traditional quasi-Landau spacing in energy. However, the resolution of the spectrum is too poor to unambiguously identify any other structure. The additional structure marked by an asterisk may be the period-doubled peak of the leading modulation, which is also present in our data as discussed above.

For  $m^\pi = 1^-$ , however, more and better resolved spectra have been published, also measured by the Bielefeld group [see Fig. 2(b) of Main *et al.*<sup>21</sup>]. The periodic orbits  $I_2$ ,  $I_3$ , and  $I_6$  have been clearly identified. Surprisingly, the orbits  $I_4$  and  $I_5$ , present in our Fourier spectra, are absent. The orbit  $I\text{I}b_1$ , which leads to a strong peak at  $\gamma^{1/3} = 2.91$  in our data, should produce a peak at  $t_{\text{rec}} = 3.04$  in the experimental data, which is also absent. The orbits  $I\text{I}b_2$  and  $I\text{I}a_2$ , responsible for the large observed peak at  $\gamma^{1/3} = 3.19$  in our data, should produce peaks at  $t_{\text{rec}} = 3.99$  and  $3.46$ , respectively. These peaks seem to be present as noted by an asterisk near  $t_{\text{rec}} \cong 4$  and also a peak near  $t_{\text{rec}} = 3.5$ , not commented on by the authors. Further experimental investigations to clarify

TABLE III. Same as Table II, but  $\varepsilon = -0.1$ , Figs. 2(c) and 2(d).

$m^\pi = 2^+$	$\gamma_i^{1/3}$	$m^\pi = 1^-$	$S_i$	Periodic orbit
1.12			1.13	$I_1$
1.63		1.64	1.64	$I_2$
		1.90	1.92	$I_3$
		2.11	2.11	$I_4$
2.25	(2.25)		$2 \times 1.12, (2.26)$	$I_1, (I_3)$
2.40	2.39		2.41	$I\text{I}b_0$
2.73			2.74	$I\text{I}a_1$
		2.75	2.76	$I\text{I}b_1$
(2.97)	(2.96)		2.99	$I\text{I}a_2, I\text{I}b_2$
(3.10)	(3.12)		3.10	$\text{III}_1$
3.37			$3 \times 1.12$	$I_1$
3.51			3.52	$\text{III}_3$
3.80	(3.79)		3.81, 3.82	$\text{III}_8, \text{III}_7$

TABLE IV. Same as Table II, but  $\varepsilon = -0.2$ , Figs. 2(e) and 2(f).

$m^\pi = 2^+$	$\gamma_i^{1/3}$	$m^\pi = 1^-$	$S_i$	Periodic orbit
1.09			1.09	$I_1$
		1.56	1.56	$I_2$
		(1.80)	1.79	$I_3$
		1.94	1.93	$I_4$
2.18			$2 \times 1.09$	$I_1$
(2.33)		2.30	2.31	$I\text{I}b_0$
2.61		2.61	2.61, 2.62	$I\text{I}a_1, I\text{I}b_1$
(3.27)			$3 \times 1.09$	$I_1$
3.37		3.39	3.35, 3.38, 3.40	$\text{III}_5, \text{III}_3, \text{III}_6$

these points are desirable.

We now turn to the  $\varepsilon$  dependence of the spectra. Quantum calculations have been performed with method C of Sec. II B. Because the generalized eigenvalue problem requires more memory, only matrices up to dimension 1296 have been diagonalized. The calculated Fourier spectra are shown in Figs. 2(c)–2(h) and are tabulated in Tables III–V. The  $\varepsilon$  dependence of the classical trajectories is smooth and is tabulated in columns 5–10 of Table I. Note that some periodic orbits no longer exist below a cutoff value  $\varepsilon_i$ . Since for  $\gamma = 0$  all periodic orbits passing through the origin are straight lines, the only periodic orbits passing through the origin which exist for all values of the magnetic field are the motions perpendicular and parallel ( $\varepsilon < 0$  only) to the field.

We will not discuss the case  $\varepsilon = -0.1$  and  $-0.2$  in detail since these cases are very similar to  $\varepsilon = 0$  (see Tables III and IV). However, we like to remark that *all* peaks appearing in the Fourier spectra can be connected to periodic orbits listed in Table I. In particular the peaks at  $\gamma^{1/3} = 2.61$  and  $2.30$  for  $\varepsilon = -0.2$  can be connected without any ambiguity to periodic orbits, which are also present in the data for  $\varepsilon > -0.02$ .

We shall discuss the case  $\varepsilon = -0.4$  in more detail. The system now has an interesting feature, namely that parts of the phase space are no longer chaotic but regular.<sup>16,23</sup>

TABLE V. Same as Table II, but  $\varepsilon = -0.4$ , Figs. 2(g) and 2(h).

$m^\pi = 2^+$	$\gamma_i^{1/3}$	$m^\pi = 1^-$	$S_i$	Periodic orbit
1.03			1.03	$I_1$
		1.41	1.41	$I_2$
2.06			$2 \times 1.03$	$I_1$
		2.11	2.12	$I\text{I}b_0$
		2.69	2.69	$\text{III}_1$
		2.80	$2 \times 1.41$	$I_2$
		2.87	2.87	$\text{III}_2$
3.10		3.10	$3 \times 1.03, 3.11$	$I_1, \text{III}_4$
		(3.30)	3.33	$\text{III}_8$
		3.52	3.52, 3.53	$\text{IV}_1, \text{IV}_2$
		4.12	4.10, 4.13	$\text{IV}_3, \text{IV}_4$
4.13			$4 \times 1.03, 4.13$	$I_1, \text{IV}_4$

Quantum mechanically this fact manifests itself in a small deviation of the nearest-neighbor spacing (NNS) distributions from a Wigner distribution.<sup>23</sup> In a more detailed analysis we find that the trajectories with initial conditions  $\dot{\mu}/\dot{\nu} > 0.65$  are regular. The regular trajectories are insensitive to small deviations of the initial conditions which propagate only linearly. The periodic orbit  $I_1$  is now stable. In addition, this orbit now has a quantum-mechanical counterpart, namely the  $K=0$  quantum states which are localized near the  $z=0$  plane and which have the smallest interaction with other quantum states.<sup>12,24</sup>

Figure 7 shows the spectra for  $\varepsilon = -0.4$ . The regularity of the  $m^\pi = -2^+$  oscillator strength distribution is obvious, although the NNS distribution is close to a Wigner function. The spectrum now consists of a small regular part including the  $K=0$  states, which carry most of the oscillator strength, overlaid by a large irregular part which is not effectively excited in dipole transitions.

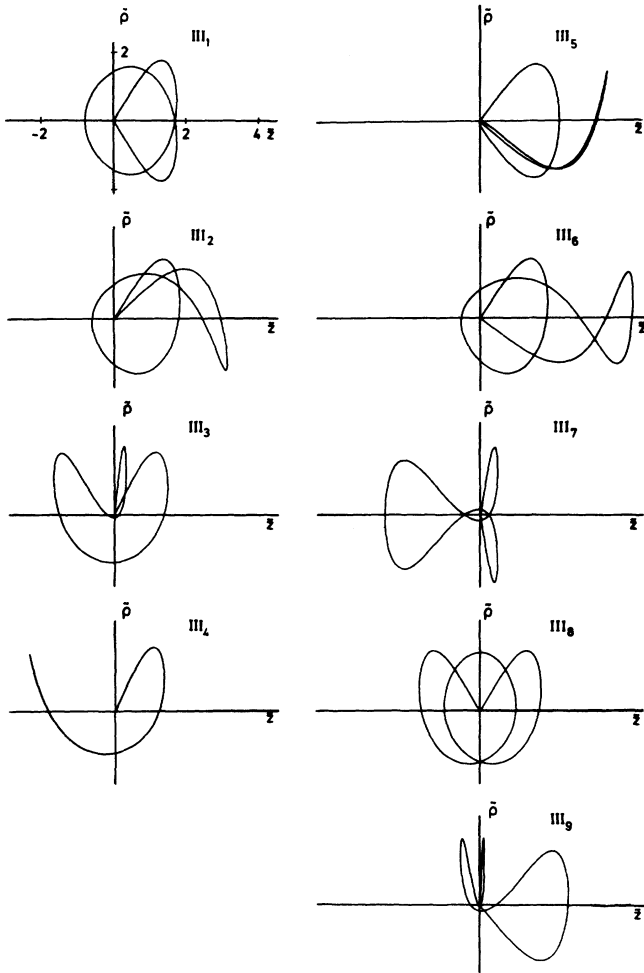


FIG. 6. Further periodic orbits at  $\varepsilon=0$  (series III). The scale is shown in the first diagram and is the same throughout the figure.

Hence the Fourier spectrum is very sparse and is dominated by the  $I_1$  orbit only, see Fig. 2(h) and Table V.

The  $m^\pi = -1^-$  spectrum looks more complicated and hence the corresponding Fourier spectrum [Fig. 2(g)] has more structure, especially around  $\gamma^{1/3} \approx 2.9$ . The peaks are tabulated in Table V. The periodic orbit  $III_4$  with  $S=3.11$ , corresponding to the very strong peak at  $\gamma^{1/3}=3.10$ , is now stable and quite insensitive to the initial conditions. Now this orbit also has a quantum counterpart, as is the case for the regular motion perpendicular to the field and the  $K=0$  states. This can be seen, e.g., in the  $m^\pi = -2^+$  spectrum, where there are satellites of the  $K=0$  states spaced at one-third of the  $K=0$  spacings, in excellent agreement with the  $S$  values of the orbits. Note, however, that these quantum states cannot be connected diabatically to low-field quantum states with a well-defined value of  $K$ ; at low fields the closest regular spacings are for motions parallel to the field (high  $K$  values) and are characterized by  $S$  values near 1.6 (see Table I) corresponding to spacings of about two-thirds of the spacings of the  $K=0$  states.

The Fourier spectrum in Fig. 2(g) contains two further strong peaks at  $\gamma^{1/3}=3.52$  and 4.12 which cannot be ex-

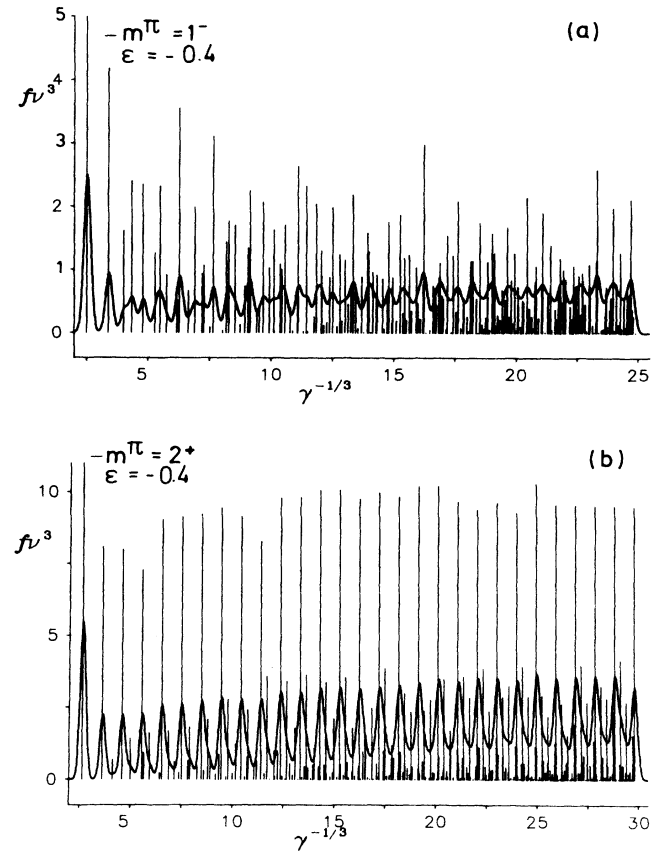


FIG. 7. Photoabsorption spectra at  $\varepsilon = -0.4$  for  $\Delta m = 0$  Balmer transitions into the  $m^\pi = -1^-$  subspace (a), and for  $\Delta m = -1$  Balmer transitions into the  $m^\pi = -2^+$  subspace (b).

plained by periodic orbits from Table I. However, there are further periodic orbits illustrated in Fig. 8 with values  $S$  ( $\epsilon = -0.4$ ) near 3.52 and 4.12. These orbits correspond to  $S$  values greater than 4 at  $\epsilon = 0$ .

Finally, we turn to a discussion of quantum-mechanical wave functions. From the discussion in this section one expects that a wave function in some sense feels the presence of periodic orbits if the resonance condition (10) is approximately fulfilled. Figure 9 shows the wave function of the quantum state in the  $m^\pi = 1^+$  subspace at  $E = 0$  and  $\gamma = 5.0412 \times 10^{-3}$ . A comparison with the periodic orbit  $I_2$  in Fig. 3 shows a large probability  $|\psi|^2$  in the vicinity of the classical trajectory; the maximum range in  $z$  of the classical orbit is roughly 76 Bohr radii and is marked by the arrow in Fig. 9. The action (10) is  $\gamma^{-1/3}S = 10.03$  which is close to an integer. Thus the

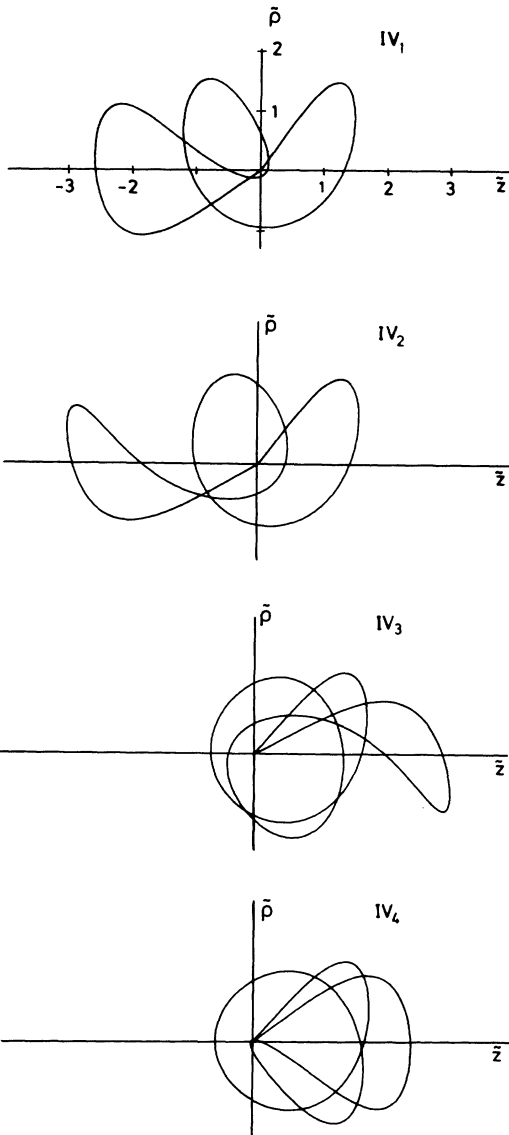


FIG. 8. Further periodic orbits at  $\epsilon = -0.4$ . The scale is shown in the first diagram and is the same throughout the figure.

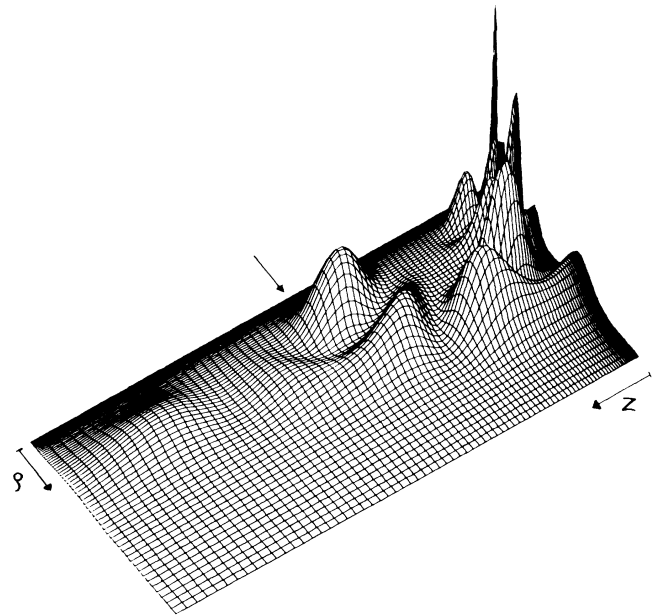


FIG. 9. Wave function  $\rho |\psi|^2$  of the eigenstate at  $E = 0$  and  $\gamma = 5.0412 \times 10^{-3}$  in the  $m^\pi = -1^+$  subspace. The arrow marks the maximum range in  $z$  ( $76a_0$ ) of the unstable periodic orbit  $I_2$  at the same energy and field strength.

wave function in Fig. 9 does appear scarred<sup>3</sup> by the presence of the periodic classical orbit.

Note, however, that in the classically chaotic regime, isolated unstable periodic orbits and individual photoabsorption peaks cannot generally be associated with individual eigenstates of the quantum Hamiltonian, as may be done when the system is regular.<sup>1</sup> The individual peaks in Fig. 8(b), at  $\epsilon = -0.4$ , are clearly associated with individual quantum  $K = 0$  states related to stable periodic orbits in the residual regular part of classical phase space. However, such an identification breaks down at  $\epsilon = 0$  [Fig. 1(b)], where the photoabsorption peaks are not individual states or resonances but merely a result of modulations of the cross sections.

#### IV. SUMMARY AND DISCUSSION

We have studied the problem of a Rydberg atom in a magnetic field classically and quantum mechanically and have investigated the correspondence between modulations in observable photoabsorption cross sections and periodic orbits in classical phase space.

Because of the scaling property of the Hamiltonian, such modulations are best studied by investigating the cross sections at fixed values of the scaled energy  $\epsilon = \gamma^{-2/3}E$  as functions of  $\gamma^{-1/3}$ . The modulations of the cross sections appear as prominent peaks in their Fourier transforms which correspond quantitatively to periodic classical orbits passing through the origin. The positions of the peaks are accurately given by the values of  $\gamma^{1/3}$  corresponding to the scaled classical action (10), which is obtained by integrating along the closed path from the origin to the first recurrence. The heights of the peaks can be

understood at least qualitatively by studying the compatibility of the geometries of the periodic classical orbits and the observed transition. A quantitative description must also include a stability analysis of the orbits. Note that most of the modulations found in this paper are predictions and await experimental verification.

The peak positions and scaled actions depend smoothly on the scaled energy  $\varepsilon$ . Many periodic orbits cease to exist below a certain cutoff energy  $\varepsilon_i$ ; at  $\gamma=0$  ( $\varepsilon=-\infty$ ) the only periodic orbits passing through the origin are straight lines. In the irregular quasi-Landau region there are several topologically different series of unstable periodic orbits. At the zero-field threshold we have found all periodic orbits passing through the origin with a scaled action  $S$  ( $\varepsilon=0$ ) less than four.

At small values of  $\varepsilon$  where classical phase space is at least partly regular, there may be a one-to-one correspondence between (stable) periodic orbits and individual quantum states dominating individual photoabsorption peaks. In this case, Eq. (9) may be interpreted as a quantization condition in the spirit of Einstein, Brillouin, and Keller.<sup>1</sup> However, around the zero-field threshold  $\varepsilon=0$  the dynamics are completely irregular and the periodic orbits are isolated and unstable. In this case Eq. (9) is

merely a resonance condition from which we can derive how a recurrence of a classical orbit leads to oscillations in the level density and hence in the cross sections. Note that the modulations corresponding to the leading peaks in the Fourier-transformed spectra contain no detailed information about the individual state-for-state structure of the quantum spectrum which is completely different in different  $m^\pi$  subspaces of final states.

The study of Rydberg atoms in an external static magnetic field is a very promising area for gaining further insights into the intriguing field of irregular dynamics. There is no need to restrict the study to atomic hydrogen, so precision measurements on other atoms<sup>37,38</sup> which are easier to handle in the laboratory would be useful. Since the scaled energy  $\varepsilon=E/\gamma^{2/3}$  is the quantity controlling the classical dynamics, measurements done by tuning the field strength  $\gamma$  at a fixed value of  $\varepsilon$ , e.g., at the zero-field threshold  $\varepsilon=0$ , would be more meaningful than spectra taken at fixed field strength.

#### ACKNOWLEDGMENT

We are grateful to the Deutsche Forschungsgemeinschaft for support and encouragement.

- <sup>1</sup>M. Berry, *Chaotic Behavior of Deterministic Systems* (North-Holland, Amsterdam, 1983), p. 172.
- <sup>2</sup>A. J. Lichtenberg and M. A. Liebermann, *Regular and Stochastic Motion* (Springer, New York, 1983); O. Bohigas and M. J. Giannoni, *Lecture Notes in Physics*, edited by T. H. Seligman and H. Nishioka (Springer, Berlin, 1986), Vol. 263, p. 18.
- <sup>3</sup>E. J. Heller, *Phys. Rev. Lett.* **53**, 1515 (1984).
- <sup>4</sup>W. R. S. Garton and F. S. Tomkins, *Astrophys. J.* **158**, 839 (1969).
- <sup>5</sup>J. C. Castro, M. L. Zimmerman, R. G. Hulet, D. Kleppner, and R. R. Freeman, *Phys. Rev. Lett.* **45**, 1780 (1980).
- <sup>6</sup>D. Delande, C. Chardonnet, F. Biraben, and J. C. Gay, *J. Phys. Paris Colloq.* **43**, C2-97 (1982).
- <sup>7</sup>A. R. Edmonds, *J. Phys. Paris Colloq.* **31**, C4-71 (1970).
- <sup>8</sup>A. R. P. Rau, *Phys. Rev. A* **16**, 613 (1977).
- <sup>9</sup>U. Fano, *Phys. Rev. A* **22**, 2260 (1980).
- <sup>10</sup>J. A. C. Gallas, F. Gerck, and R. F. O'Connell, *Phys. Rev. Lett.* **50**, 324 (1983).
- <sup>11</sup>C. W. Clark, *Atomic Excitations and Recombination in External Fields*, edited by M. H. Nayfeh and C. W. Clark (Gordon and Breach, London, 1985); M. A. Al Laithy, P. F. O'Mahony, and K. T. Taylor, *J. Phys. B* **19**, L773 (1986).
- <sup>12</sup>D. Wintgen and H. Friedrich, *J. Phys. B* **19**, L99 (1986).
- <sup>13</sup>W. P. Reinhardt, *J. Phys. B* **16**, L635 (1983).
- <sup>14</sup>M. Robnik, *J. Phys. A* **14**, 3195 (1981).
- <sup>15</sup>J. B. Delos, S. K. Knudson, and D. W. Noid, *Phys. Rev. A* **30**, 1208 (1984).
- <sup>16</sup>A. Harada and H. Hasegawa, *J. Phys. A* **16**, L259 (1983); H. Hasegawa, S. Adachi, and A. Harada, *J. Phys. A* **16**, L503 (1983).
- <sup>17</sup>D. Wintgen and H. Friedrich, *Phys. Rev. Lett.* **57**, 571 (1986).
- <sup>18</sup>D. Delande and J. C. Gay, *Phys. Rev. Lett.* **57**, 2006 (1986).
- <sup>19</sup>G. Wunner, U. Woelk, I. Zech, G. Zeller, T. Ertl, F. Geyer, W. Schweizer, and H. Ruder, *Phys. Rev. Lett.* **57**, 3261 (1986).
- <sup>20</sup>A. Holle, G. Wiebusch, J. Main, B. Hager, H. Rottke, and K. H. Welge, *Phys. Rev. Lett.* **56**, 2594 (1986).
- <sup>21</sup>J. Main, G. Wiebusch, A. Holle, and K. H. Welge, *Phys. Rev. Lett.* **57**, 2789 (1986).
- <sup>22</sup>D. Wintgen, A. Holle, G. Wiebusch, J. Main, H. Friedrich, and K. H. Welge, *J. Phys. B* **19**, L557 (1986).
- <sup>23</sup>D. Wintgen and H. Friedrich, *Phys. Rev. A* **35**, 1464 (1987).
- <sup>24</sup>D. Wintgen and H. Friedrich, *J. Phys. B* **19**, 1261 (1986).
- <sup>25</sup>D. Wintgen and H. Friedrich, *J. Phys. B* **19**, 991 (1986).
- <sup>26</sup>D. Delande and J. C. Gay, *J. Phys. B* **19**, L173 (1986).
- <sup>27</sup>C. W. Clark and K. T. Taylor, *J. Phys. B* **13**, L737 (1980), **15**, 1175 (1982).
- <sup>28</sup>P. F. O'Mahony and K. T. Taylor, *J. Phys. B* **19**, L65 (1986).
- <sup>29</sup>G. Wunner, M. Kost, and H. Ruder, *Phys. Rev. A* **33**, 1444 (1986).
- <sup>30</sup>E. A. Solov'ev, *Pis'ma Zh. Eksp. Teor. Fiz.* **34**, 278 (1981) [*JETP Lett.* **34**, 265 (1981)].
- <sup>31</sup>J. B. Delos, S. K. Knudson, and D. W. Noid, *Phys. Rev. Lett.* **50**, 579 (1983); *Phys. Rev. A* **28**, 7 (1983).
- <sup>32</sup>M. L. Zimmerman, M. M. Kash, and D. Kleppner, *Phys. Rev. Lett.* **45**, 1092 (1980).
- <sup>33</sup>E. J. Heller, *J. Chem. Phys.* **65**, 4979 (1976).
- <sup>34</sup>D. Wintgen, *Phys. Rev. Lett.* **58**, 1589 (1987).
- <sup>35</sup>S. Feneuille, *Phys. Rev. A* **26**, 673 (1982).
- <sup>36</sup>H.-D. Meyer, *J. Chem. Phys.* **84**, 3147 (1986); D. Wintgen (unpublished).
- <sup>37</sup>H. Rinneberg, J. Neukammer, G. Jönsson, H. Hieronymus, A. König, and K. Vietzke, *Phys. Rev. Lett.* **55**, 382 (1985).
- <sup>38</sup>P. Cacciani, E. Luc-Koenig, J. Pinard, C. Thomas, and S. Liberman, *J. Phys. B* **19**, L519 (1986).